Stokes-Correlometry Analysis of Biological Tissues with Polycrystalline Structure

Alexander Ushenko, Anton Sdobnov, Alexander Dubolazov, Marta Gritsuk, Yurii Ushenko, Alexander Bykov, and Igor Meglinski*, Senior Member, IEEE

Abstract—Utilizing Stokes-correlometry analysis a new diagnostic approach has been introduced for quantitative assessment of polarization images of histological sections of optically anisotropic biological tissues with different morphological structures and physiological conditions. The developed approach is based on the quantitative assessment of coordinate and phase distributions of the Stokes vector of scattered light. A combined use of statistic, correlation and fractal analysis is used for resolving variations in optical anisotropy of biological samples. The proposed combined application of the statistical, correlation and fractal-based evaluates of spatial distributions of 'single-point' polarization azimuth, ellipticity and 'two-point' Stokes vector parameters of polarization images of biological tissues histological sections demonstrates a high accuracy ($Ac \geq 90\%$) in monitoring of optical anisotropy variations within biological tissues.

Index Terms—Polarimetric imaging, polarization, ellipsometry and polarimetry, Stokes-correlometry.

I. INTRODUCTION

THE optically-based polarimetry is popular experimental approach widely used for non-invasive diagnosis of various turbid tissue-like scattering media [1-6], including those containing optically anisotropic layers [7-9] and fluids [10-12]. With the recent instrumentation developments in the field, a high sensitivity of laser polarimetry in screening of turbid cancerous biological tissues has been achieved [13-16]. The further development of this approach is based on the statistical analysis of averaged values of the polarization parameters (e.g. such as polarization azimuth and ellipticity), obtained for a wide range of variations in the selected samples

A.G. Ushenko, A.V. Dubolazov, M. Gritsuk and Yu.A. Ushenko are with the Chernivtsi National University, 2 Kotsiubynskyi St., Chernivtsi, Ukraine.A.Yu. Sdobnov, A. Bykov with the Opto-Electronic and Measurement Techniques, University of Oulu, P.O. Box 4500, Oulu, 90014, Finland.

* I. Meglinski with the Opto-Electronic and Measurement Techniques, University of Oulu, P.O. Box 4500, Oulu, 90014, Finland; Interdisciplinary Laboratory of Biophotonics, National Research Tomsk State University, Tomsk, 634050, Russia; National Research Nuclear University "MEPhI", Institute of Engineering Physics for Biomedicine (PhysBio), 115409 Moscow, Russia (Correspondence: e-mail: igor.meglinski@oulu.fi and tel.: +358294488888).

of biological tissues from the series of microscopy images [3-5,17]. The major application in frame of these studies has been focused on the diagnosis of the biological tissues at different stage of cancer as well as pre-cancerous human tissues with fibrillar structure of polycrystalline networks. Pathological malformations in such tissues are typically accompanied by a significant changes in the phase anisotropy and/or birefringence properties due to the spatial transformation of optical axes of the protein fibrils [4,18,19]. It has been demonstrated that statistical analysis of 'one-point' spatial distributions of the polarization azimuth and ellipticity values, obtained from microscopy images of optically thin tissues, as well as the analysis of polycrystalline layers of biological fluids, are quite effective when an assessment of pathological progression is required [10-12,18,19]. The disadvantage of this approach is the lack of data corresponding to the spatial consistency (degree of correlation) of the polarization parameters at different points in the phase-inhomogeneous object field of biological layers. The theoretical basis for obtaining such data is presented in Ref. [20]. Here, a new analytical parameter – the complex degree of mutual polarization (CDMP) is introduced to characterize the correlation structure of polarization-inhomogeneous fields. CDMP characterizes the correlation consistency degree of polarization states (azimuth and ellipticity) at various points of the optical field. This theoretical polarization-correlation approach has been generalized in frames of the polycrystalline structure analysis. Further, this method has been successfully experimentally tested for differentiation of pathological changes in their optical anisotropy [21-26]. Also, the generalization of the CDMP-analysis of polarization-inhomogeneous object fields of biological layers using the "two-point" formalism of the Stokes vector has been theoretically introduced in [27,28]. However, a number of unsolved problems remain in the field of polarization correlometry:

i. the absence of a unified experimental methodology for the parameters distributions mapping on the basis of the synthesis of traditional Stokes-Polarimetry and Stokes-correlometry;

ii. the possibility of diagnostics of weak changes in optical anisotropy of a more wider (comparing to the fibrillar) morphological class of biological tissues.

The importance of these problems solving is due to the fact that in reality, the most of human organs, including liver, stomach, pancreas, spleen, and lungs, have a parenchymal structure, when optical anisotropy are formed by spatially separated within the tissue localized areas. The polarization

changes associated with birefringence for such optically heterogeneous structure are very small. Therefore, the application of mentioned above statistical approach for such tissue samples is less effective. Thus, further developments of optical polarimetry for tissue diagnosis focused on screening of the parenchymatous tissues and quantitative assessment of the optical anisotropy changes associated with malformations of tissues are expected.

In current paper we present the fundamentals behind of the laser Stokes-polarimetry approach and consider its application, utilizing polarization-correlation mapping of microscopy images of the histological sections of parenchymatous biological tissues, determining the spatial distribution of 'two-point' Stokes vector parameters.

II. THEORY OF THE METHOD

The following assumptions are based on the theoretical model of the Stokes-correlometry method of polarization-inhomogeneous object fields of biological tissues layers:

1. To describe the correlation structure of the stationary distributions of the fields of complex amplitudes of laser light converted by optically anisotropic biological layers, the following mutual spectral density matrix is used [27,28]:

$$W_{i,j}(r_1, r_2) = E_i^*(r_1) \cdot E_j(r_2), i, j = x, y. \tag{1}$$

Here, r_1 and r_2 are the coordinates of the neighboring points in the laser radiation field.

Using this matrix operator the following expression for the "two-point" Stokes vector parameters can be obtained:

$$S_1 = W_{xx}(r_1, r_2) + W_{yy}(r_1, r_2), \tag{2}$$
$$S_2 = W_{xx}(r_1, r_2) - W_{yy}(r_1, r_2), \tag{3}$$
$$S_3 = W_{xy}(r_1, r_2) - W_{yx}(r_1, r_2), \tag{4}$$
$$S_4 = i\left[W_{yx}(r_1, r_2) + W_{xy}(r_1, r_2)\right] \tag{5}$$

where,

$$\begin{cases} W_{xx}(r_1, r_2) = E_x^*(r_1)E_x(r_2); \\ W_{yy}(r_1, r_2) = E_y^*(r_1)E_y(r_2); \\ W_{xy}(r_1, r_2) = E_x^*(r_1)E_y(r_2); \\ W_{yx}(r_1, r_2) = E_y^*(r_1)E_x(r_2). \end{cases} \tag{6}$$

Using relations (2)–(6) the following equations for "two-point" Stokes vector parameters (hereinafter Stokes-correlometry parameters – SCP) calculation can be obtained:

$$S_1(r_1, r_2) = E_x^*(r_1)E_x(r_2) + E_y^*(r_1)E_y(r_2); \tag{7}$$
$$S_2(r_1, r_2) = E_x^*(r_1)E_x(r_2) - E_y^*(r_1)E_y(r_2); \tag{8}$$
$$S_3(r_1, r_2) = E_x^*(r_1)E_y(r_2) + E_y^*(r_1)E_x(r_2); \tag{9}$$
$$S_4(r_1, r_2) = i\left[E_y^*(r_1)E_x(r_2) - E_x^*(r_1)E_y(r_2)\right]. \tag{10}$$

2. Let us consider the object field of an optically anisotropic biological layer. The complex amplitudes $E(r)$ of each point r of such a field are described by Jones vector [4,26]:

$$E(r) = \begin{pmatrix} E_x \\ E_y \end{pmatrix}(r) = \begin{pmatrix} |E_x| \\ |E_y|\exp(\delta_y - \delta_x) \end{pmatrix}(r) = \tag{11}$$
$$= \begin{pmatrix} 1 \\ tg\rho\exp(\delta) \end{pmatrix}(r) = \begin{pmatrix} 1 \\ tg\rho(\cos\delta + i\sin\delta) \end{pmatrix}(r)$$

Here, $tg\rho(r) = \dfrac{|E_y|(r)}{|E_x|(r)}$ and $\delta(r) = (\delta_y - \delta_x)(r)$ is the phase shift between the orthogonal components ($|E_x|(r), |E_y|(r)$) of laser wave amplitude.

3. Taking into account (11) the equations (7) – (10) can be rewritten as:

$$S_1(r_1, r_2) = (1 + tg\rho_1 tg\rho_2 \cos(\delta_1 - \delta_2)) - i(tg\rho_1 tg\rho_2 \sin(\delta_1 - \delta_2)); \tag{12}$$

$$S_2(r_1, r_2) = (1 - tg\rho_1 tg\rho_2 \cos(\delta_1 - \delta_2)) + i(tg\rho_1 tg\rho_2 \sin(\delta_1 - \delta_2)); \tag{13}$$

$$S_3(r_1, r_2) = (tg\rho_2 \cos\delta_2 + tg\rho_1 \cos\delta_1) + i(tg\rho_2 \sin\delta_2 - tg\rho_1 \sin\delta_1); \tag{14}$$

$$S_4(r_1, r_2) = (tg\rho_1 \sin\delta_1 + tg\rho_2 \sin\delta_2) + i(tg\rho_1 \cos\delta_1 - tg\rho_2 \cos\delta_2). \tag{15}$$

4. Based on (12) – (15), the expressions for the experimentally measured components of the complex parameters of the 'two-point' parameters of the Stokes vector the modulus $S_{i=1;2;3;4}(r_1, r_2)$ and phase $ArgS_{i=1;2;3;4}$ - $|S_{i=1;2;3;4}|$ have been defined as:

$$\begin{cases} |S_1|(r_1, r_2) = ((1 + tg\rho_1 tg\rho_2 \cos(\delta_1 - \delta_2))^2 + (tg\rho_1 tg\rho_2 \sin(\delta_1 - \delta_2))^2)^{0.5}; \\ ArgS_2(r_1, r_2) = arctg\left(\dfrac{tg\rho_1 tg\rho_2 \sin(\delta_1 - \delta_2)}{(1 + tg\rho_1 tg\rho_2 \cos(\delta_1 - \delta_2))}\right); \end{cases} \tag{16}$$

$$\begin{cases} |S_2|(r_1, r_2) = ((1 - tg\rho_1 tg\rho_2 \cos(\delta_1 - \delta_2))^2 + (tg\rho_1 tg\rho_2 \sin(\delta_1 - \delta_2))^2)^{0.5}; \\ ArgS_2(r_1, r_2) = arctg\left(\dfrac{tg\rho_1 tg\rho_2 \sin(\delta_1 - \delta_2)}{(1 - tg\rho_1 tg\rho_2 \cos(\delta_1 - \delta_2))}\right); \end{cases} \tag{17}$$

$$\begin{cases} |S_3|(r_1, r_2) = ((tg\rho_2 \cos\delta_2 + tg\rho_1 \cos\delta_1)^2 + (tg\rho_2 \sin\delta_2 - tg\rho_1 \sin\delta_1)^2)^{0.5}; \\ ArgS_3(r_1, r_2) = arctg\left(\dfrac{(tg\rho_2 \sin\delta_2 - tg\rho_1 \sin\delta_1)}{(tg\rho_2 \cos\delta_2 + tg\rho_1 \cos\delta_1)}\right); \end{cases} \tag{18}$$

$$\begin{cases} |S_4|(r_1, r_2) = ((tg\rho_1 \sin\delta_1 + tg\rho_2 \sin\delta_2)^2 + (tg\rho_1 \cos\delta_1 - tg\rho_2 \cos\delta_2)^2)^{0.5}; \\ ArgS_4(r_1, r_2) = arctg\left(\dfrac{(tg\rho_1 \cos\delta_1 - tg\rho_2 \cos\delta_2)}{(tg\rho_1 \sin\delta_1 + tg\rho_2 \sin\delta_2)}\right). \end{cases} \tag{19}$$

5. Further, for simplification (without affecting the completeness of analysis) relations (16)–(19) can be considered in the approximation of weak phase modulation ($\delta_i \leq 0,12 rad$; $\cos\delta_i \to 1$; $\sin\delta_i \to \delta_i$). Important to note that this assumption is not artificial for optically thin histological sections of rat kidney and liver. It can be shown that for laser light with the wavelength $\lambda = 0.63\mu m$ within

geometric thickness $l = 30 \mu m$ of completely optically anisotropic layer in biological tissue ($\Delta n \approx 10^{-4} \div 1.5 \times 10^{-3}$ [28]) the maximal phase shift ($\delta_{12} \equiv \delta = \frac{2\pi}{\lambda} \Delta n l$) takes values $0.03 rad \leq \delta \leq 0.45 rad$. Moreover, among the birefringent networks or "islets" (clusters of spatially non-oriented protein molecules) there are variations of transverse dimensions of birefringent ($2 \mu m \leq \Delta l \leq 20 \mu m$) structures, which forms weak phase modulations ($0.002 rad \leq \Delta\delta \leq 0.3 rad$) in the polarization-inhomogeneous image plane. Under these conditions Eqs.(16) – (19) can be modified as:

$$\begin{cases} |S_1|(r_1, r_2) = \left((1 + tg\rho_1 tg\rho_2)^2 + (tg\rho_1 tg\rho_2(\delta_1 - \delta_2))^2\right)^{0.5}; \\ ArgS_2(r_1, r_2) = arctg\left(\frac{tg\rho_1 tg\rho_2(\delta_1 - \delta_2)}{(1 + tg\rho_1 tg\rho_2)}\right); \end{cases} \quad (20)$$

$$\begin{cases} |S_2|(r_1, r_2) = \left((1 - tg\rho_1 tg\rho_2)^2 + (tg\rho_1 tg\rho_2(\delta_1 - \delta_2))^2\right)^{0.5}; \\ ArgS_2(r_1, r_2) = arctg\left(\frac{tg\rho_1 tg\rho_2(\delta_1 - \delta_2)}{(1 - tg\rho_1 tg\rho_2)}\right); \end{cases} \quad (21)$$

$$\begin{cases} |S_3|(r_1, r_2) = \left((tg\rho_2 + tg\rho_1)^2 + (\delta_2 tg\rho_2 - \delta_1 tg\rho_1)^2\right)^{0.5}; \\ ArgS_3(r_1, r_2) = arctg\left(\frac{(\delta_2 tg\rho_2 - \delta_1 tg\rho_1)}{(tg\rho_2 + tg\rho_1)}\right); \end{cases} \quad (22)$$

$$\begin{cases} |S_4|(r_1, r_2) = \left((\delta_1 tg\rho_1 + \delta_2 tg\rho_2)^2 + (tg\rho_1 - tg\rho_2)^2\right)^{0.5}; \\ ArgS_4(r_1, r_2) = arctg\left(\frac{(tg\rho_1 - tg\rho_2)}{(\delta_1 tg\rho_1 + \delta_2 tg\rho_2)}\right). \end{cases} \quad (23)$$

The analysis of the obtained relations (20) – (23) revealed:

i. in case of weak phase fluctuations $\delta_{1;2}$ the value $|S_{1-4}|(r_1, r_2)$ are predominantly determined by the components which are functionally depends on the parameters $\rho_{1;2}$;

ii. the value $ArgS_{1-4}(r_1, r_2)$ has a complex dependence on $\delta_{1;2}$ and $\rho_{1;2}$ in the points of the object field of the optically anisotropic biological layer.

6. The detailed analytical and experimental analysis of the polarimetry of the 3rd and the 4th 'two-point' Stokes vector parameters can be potentiality is used in further experiments. This assumption is based on the fact that the first Stokes-vector parameter $S_1(r)$ characterizes the full intensity at the point r, while the second $S_2(r)$ and the third $S_3(r)$ parameters are responsible for the characterization of the changes in polarization azimuth and ellipticity. The fourth Stokes-vector parameter $S_4(r)$ characterizes the value of polarization ellipticity.

Let us define the characteristic values and ranges of the values of the 3rd and the 4th parameters of the two-point Stokes vector, as well as their modulus and phase. As an object of study, we consider an optically anisotropic biological layer. It forms the value of the phase shift $\delta(r)$ and the ratio $\rho(r)$ between the orthogonal components of the amplitude

$|E_x|(r), |E_y|(r)$. Let us consider (without reducing the completeness of the analysis) that such a layer is illuminated by the linearly polarized beam with azimuth – 0^0 ($E_0 = \begin{pmatrix} 1 \\ 0 \end{pmatrix}$).

Table I presents the characteristic values of the "two-point" parameters $S_{3;4}(r_1, r_2)$ (relations (7) - (15)) and components of the Stokes vector $|S_4|(r_1, r_2)$ and $ArgS_{3;4}(r_1, r_2)$ (relations (17) - (19)) for different polarization states at the points r, r_2 of the object field of such a layer.

The data given in Table 1 determines the range of variation of the parameters $|S_{3;4}|(r_1, r_2)$ and $ArgS_{3;4}(r_1, r_2)$, depending on the change in the coordinate structure (r_1, r_2) of the polarization states ($\rho_{1;2}, \delta_{1;2}$) of the object field of the optically anisotropic layer:

$$0 \leq |S_{3;4}|(r_1, r_2) \leq 1; \quad (24)$$
$$0 \leq ArgS_{3;4}(r_1, r_2) \leq 0.5\pi. \quad (25)$$

Further, the coordinate ($\Delta r \equiv \Delta x; \Delta y$) distributions $|S_{i=3;4}(\Delta x; \Delta y)|$ will be called SCP "orientation maps", and $Arg(S_{i=3;4}(\Delta x; \Delta y))$ - the SCP phase maps.

The described assumptions will be used for the analysis of experimental data of the Stokes-correlometry method of object fields of histological sections of real biological tissues.

III. METHOD AND MATERIALS

Measurements of the coordinate distributions of the values of parameters $|S_{i=3}(\Delta x; \Delta y)|$, $Arg(S_{i=3}(\Delta x; \Delta y))$, $|S_{i=4}(\Delta x; \Delta y)|$, and $Arg(S_{i=4}(\Delta x; \Delta y))$ were carried out in the experimental arrangement of Stokes-polarimeter. Fig.1 demonstrates the optical scheme of the Sokes-polarimeter [4,18,19].
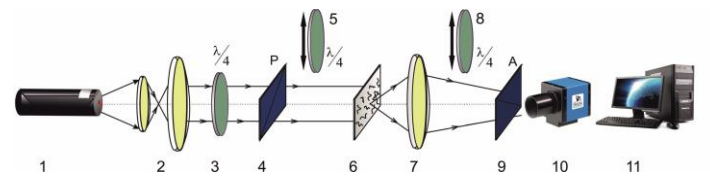
Fig. 1. Optical scheme of polarimeter, where: 1 - He-Ne laser; 2 - collimator; 3 - stationary quarter-wave plate; 5, 8 - mechanically movable quarter-wave plates; 4, 9 - polarizer and analyzer; 6 - biological layer; 7 - polarizing microobjective; 10 - CCD camera; 11 – PC.

Biological tissue sample were illuminated by parallel ($\varnothing = 2 \times 10^3 \mu m$) low-intensity (W = 5.0 мW) He-Ne laser (λ=0,6328 μm, Laser, Edmund Optics, USA). Polarization light-source consists of quarter-wave plate (Achromatic True Zero-Order Waveplate (APAW 15 mm, Astropribor, Ukraine) and polarizer (B + W XS-Pro Polarizer MRC Nano, Kaesemann, Germany).

TABLE I.

CHARACTERISTIC VALUES OF THE MODULUS $|S_4|(r_1,r_2)$ AND PHASE $ArgS_{3;4}(r_1,r_2)$ OF THE "TWO-POINT" PARAMETERS $S_{3;4}(r_1,r_2)$ OF THE STOKES VECTOR OF THE POLARIZATION-INHOMOGENEOUS OBJECT FIELD OF AN OPTICALLY ANISOTROPIC BIOLOGICAL LAYER

$\rho_1, rad;$ δ_1, rad	$E(r_1)$	$\rho_2, rad;$ δ_2, rad	$E(r_2)$	$|S_3|(r_1,r_2)$	$ArgS_3(r_1,r_2)$	$|S_4|(r_1,r_2)$	$ArgS_4(r_1,r_2)$
"Collinear" states of polarization in points r_1, r_2							
$\rho_1 = 0;$ $\delta_1 = 0$	$\begin{pmatrix}1\\0\end{pmatrix}$	$\rho_2 = 0;$ $\delta_2 = 0$	$\begin{pmatrix}1\\0\end{pmatrix}$	0	"-"	0	"-"
$\rho_1 = 0.25\pi;$ $\delta_1 = 0$	$\frac{1}{\sqrt{2}}\begin{pmatrix}1\\1\end{pmatrix}$	$\rho_2 = 0.25\pi;$ $\delta_2 = 0$	$\frac{1}{\sqrt{2}}\begin{pmatrix}1\\1\end{pmatrix}$	1	0	0	"-"
$\rho_1 = 0.25\pi;$ $\delta_1 = 0.5\pi$	$\frac{1}{\sqrt{2}}\begin{pmatrix}1\\i\end{pmatrix}$	$\rho_2 = 0.25\pi;$ $\delta_2 = 0.5\pi$	$\frac{1}{\sqrt{2}}\begin{pmatrix}1\\i\end{pmatrix}$	1	0	1	0
"Intermediate" states of polarization in points r_1, r_2							
$\rho_1 = 0;$ $\delta_1 = 0$	$\begin{pmatrix}1\\0\end{pmatrix}$	$\rho_2 = 0.25\pi;$ $\delta_2 = 0$	$\frac{1}{\sqrt{2}}\begin{pmatrix}1\\1\end{pmatrix}$	$\frac{1}{\sqrt{2}}$	0	$\frac{1}{\sqrt{2}}$	0.5π
$\rho_1 = 0.5\pi;$ $\delta_1 = 0$	$\begin{pmatrix}1\\0\end{pmatrix}$	$\rho_2 = 0.25\pi;$ $\delta_2 = 0$	$\frac{1}{\sqrt{2}}\begin{pmatrix}1\\1\end{pmatrix}$	$\frac{1}{\sqrt{2}}$	0	$\frac{1}{\sqrt{2}}$	0.5π
$\rho_1 = 0;$ $\delta_1 = 0$	$\begin{pmatrix}1\\0\end{pmatrix}$	$\rho_2 = 0.25\pi;$ $\delta_2 = 0.5\pi$	$\frac{1}{\sqrt{2}}\begin{pmatrix}1\\i\end{pmatrix}$	$\frac{1}{\sqrt{2}}$	0	$\frac{1}{\sqrt{2}}$	0.5π
"Orthogonal" states of polarization in points r_1, r_2							
$\rho_1 = 0;$ $\delta_1 = 0$	$\begin{pmatrix}1\\0\end{pmatrix}$	$\rho_2 = 0.5\pi;$ $\delta_2 = 0$	$\begin{pmatrix}0\\1\end{pmatrix}$	1	0	1	0.5π
$\rho_1 = 0.25\pi;$ $\delta_1 = 0$	$\frac{1}{\sqrt{2}}\begin{pmatrix}1\\1\end{pmatrix}$	$\rho_2 = -0.25\pi;$ $\delta_2 = 0$	$\frac{1}{\sqrt{2}}\begin{pmatrix}1\\-1\end{pmatrix}$	0	"-"	1	0.5π
$\rho_1 = 0.25\pi;$ $\delta_1 = 0.5\pi$	$\frac{1}{\sqrt{2}}\begin{pmatrix}1\\i\end{pmatrix}$	$\rho_2 = 0.25\pi;$ $\delta_2 = -0.5\pi$	$\frac{1}{\sqrt{2}}\begin{pmatrix}1\\-i\end{pmatrix}$	0	"-"	0	"-"

Polarization images of biological layer were projected into the plane of the light-sensitive plate ($m \times n = 1280 \times 960$ pixels) of CCD-camera (DMK 41AU02.AS, The Imaging Source, Germany) by polarization microobjective (CFI Achromat P, focal length - 30 mm, numerical aperture - 0.1 increase - 4×, Nikon, Japan).

Analysis of the images of biological layers 6 was carried out using polarizer and the quarter-wave plate (see Fig.1).

The measuring method for the modulus $|(S_{i=3;4}(\Delta x, \Delta y))|$ and the phase $Arg(S_{i=3;4}(\Delta x, \Delta y))$ of the SCP consists of the following steps:

i. Biological tissue sample is illuminated by circularly polarized laser beam, passed through the quarter-wave plates and polarizer (see Fig.1);

ii. The axis of polarizer-analyzer (in the absence of the quarter wavelength plate) is rotated by the angles $\Theta = 0^0$, $\Theta = 90^0$, $\Theta = 45^0$, $\Theta = 135^0$. The intensities of transmitted radiation $I_0^\otimes; I_{90}^\otimes; I_{45}^\otimes; I_{135}^\otimes$ are measured;

iii. The values of the first, second and third Stokes vector parameters $S_{i=1;2;3}^\otimes$ - $S_1^\otimes = I_0^\otimes + I_{90}^\otimes$; $S_2^\otimes = I_0^\otimes - I_{90}^\otimes$; $S_3^\otimes = I_{45}^\otimes - I_{135}^\otimes$ are calculated within each pixel of digital camera (see Fig.1).

iv. Quarter-wave plate is placed in front of polarizer-analyzer, which axis of a greatest speed being oriented at the angles $+45^0$ and -45^0 relative to the transmission plane of polarizer. The intensities $I_\otimes^\otimes; I_\oplus^\otimes$ of the transmitted radiation is measured.

v. 2-dimensional array of values of the fourth Stokes parameter $S_4^\otimes = I_\otimes^\otimes - I_\oplus^\otimes$ is calculated.

vi. $|S_{i=3}(\Delta x; \Delta y)|$, $Arg(S_{i=3}(\Delta x; \Delta y))$, $|S_{i=4}(\Delta x; \Delta y)|$, and $Arg(S_{i=4}(\Delta x; \Delta y))$ are calculated utilizing the following ratios:

$$|S_3| = \sqrt{ \begin{array}{l} \left[\sqrt{I_0(r_1)I_{90}(r_2)}\cos\delta_2 + \atop + \sqrt{I_0(r_2)I_{90}(r_1)}\cos\delta_1 \right]^2 + \\ + \left[\sqrt{I_0(r_1)I_{90}(r_2)}\sin\delta_2 - \atop - \sqrt{I_0(r_2)I_{90}(r_1)}\sin\delta_1 \right]^2 \end{array} } ;$$

$$ArgS_3 = arctg\left(\frac{ \left[\sqrt{I_0(r_1)I_{90}(r_2)}\sin\delta_2 - \atop - \sqrt{I_0(r_2)I_{90}(r_1)}\sin\delta_1 \right] }{ \left[\sqrt{I_0(r_1)I_{90}(r_2)}\cos\delta_2 + \atop + \sqrt{I_0(r_2)I_{90}(r_1)}\cos\delta_1 \right] } \right). \tag{26}$$

$$|S_4| = \sqrt{ \begin{array}{l} \left[\sqrt{I_0(r_2)I_{90}(r_1)}\sin\delta_1 + \atop + \sqrt{I_0(r_1)I_{90}(r_2)}\sin\delta_2 \right]^2 + \\ + \left[\sqrt{I_0(r_2)I_{90}(r_1)}\cos\delta_2 + \atop + \sqrt{I_0(r_1)I_{90}(r_2)}\cos\delta_1 \right]^2 \end{array} } ;$$

$$ArgS_4 = arctg\left(\frac{ \left[\sqrt{I_0(r_2)I_{90}(r_1)}\cos\delta_2 + \atop + \sqrt{I_0(r_1)I_{90}(r_2)}\cos\delta_1 \right] }{ \left[\sqrt{I_0(r_2)I_{90}(r_1)}\sin\delta_1 + \atop + \sqrt{I_0(r_1)I_{90}(r_2)}\sin\delta_2 \right] } \right). \tag{27}$$

$$\delta(r) = arctg\left[\left(\frac{S_4(r)S_2(r)}{S_3(r)} \right) \left(\frac{1 + \frac{I_{90}(r)}{I_0(r)}}{1 - \frac{I_{90}(r)}{I_0(r)}} \right) \right]. \tag{28}$$

Here I_0 and are the intensities of polarizer transmission plane at 0^0 and 90^0 orientation; δ_i is the phase shift between the orthogonal components of the laser radiation amplitude in the points with coordinates r_1 and r_2.

Optically thin (attenuation coefficient $\tau = 0.01$) histological sections of biological tissues (thickness $l = 25\mu m \div 30\mu m$ $0.0093 \le \tau \le 0.0099$) taken from two statistically significant (39 samples each) groups of rats healthy and diabetic ones (21 days) were examined:
• kidney tissue – structured tissue with optically anisotropic birefringent collagen network;
• liver tissue – parenchymatous tissue with disordered optically anisotropic protein "islets".
Histological sections of tissue samples were prepared by standard freezing microtome approach.

A. Statistical analysis

To assess the distribution of random values of $q = \begin{cases} |S_{i=3;4}(\Delta x; \Delta y)| \\ Arg(S_{i=3;4}(\Delta x; \Delta y)) \end{cases}$ a set of statistical moments of the 1st to 4th order is calculated [4,18,19].

$$Z_1 = \frac{1}{N}\sum_{i=1}^{N}|(q)_i|; Z_2 = \sqrt{\frac{1}{N}\sum_{i=1}^{N}(q)_i^2};$$
$$Z_3 = \frac{1}{Z_2^3}\frac{1}{N}\sum_{i=1}^{N}(q)_i^3; Z_4 = \frac{1}{Z_2^4}\frac{1}{N}\sum_{i=1}^{N}(q)_i^4. \tag{29}$$

Here, N is the number (1280×960) of pixel at the digital camera.

B. Correlation analysis

To calculate the average value within all n lines (1, ... , m) of the photosensitive plate of CCD-camera (see Fig.1) the autocorrelation function $\overline{K}(\Delta x)$ with scanning step $\Delta x = 1pix$ of distributions of the q parameters values was used [9,13,17]:

$$K_{j=1\div n}(\Delta x) = \lim_{x \to 0}\frac{1}{m}\int_0^x \left[q_j^*(x = 1 \div m) \right]\left[q^*(x - \Delta x) \right]dx. \tag{30}$$

Here, $\overline{q}$ is the average value of the set q.

$$\overline{K}(\Delta x) = \sum_{j=1}^{n}\frac{K_j(\Delta x)}{n}. \tag{31}$$

C. Fractal analysis

Fractal analysis was performed by calculating the logarithmic dependences ($\log J(q) - \log(\nu)$) of power spectra of random values q distributions. Here $\nu = d^{-1}$ is the spatial frequencies defined by the geometrical size (d) of the structural elements of SCS-maps of the polarization-inhomogeneous image of the biological layer. Then, dependences $\log J(q) - \log(\nu)$ are approximated into curves $\Phi(\eta)$ by least squares method. The classification of the coordinate distributions was performed by the appearance of the obtained curves [4,18,19]:
• distributions of q - fractal at a constant inclination angle $\eta = const$ of the dependence $\Phi(\eta)$ for 2-3 decades of the size change d;
• distributions of q - multifractal under the condition of several constant inclination angles $\Phi(\eta)$;
• distributions of q - random under the condition of the absence of stable inclination angles throughout the range of the size change d;
The 2-nd order statistical moment has been selected as one of the parameters characterizing the distribution of $\log J(q) - \log(\nu)$ dependence values:

Fig.2. Maps (coordinate distributions (1), (5), histograms (2), (6), autocorrelation functions (3), (7), logarithmic dependences of power spectra (4), (8)) of SCP modulus $\left|S_{i=3}\left(\Delta x;\Delta y\right)\right|$ of polarization-inhomogeneous images of histological sections of a healthy ((1), (2), (3), (4)) and pathologically changed ((5), (6), (7), (8)) rat kidney. See explanations in the text.
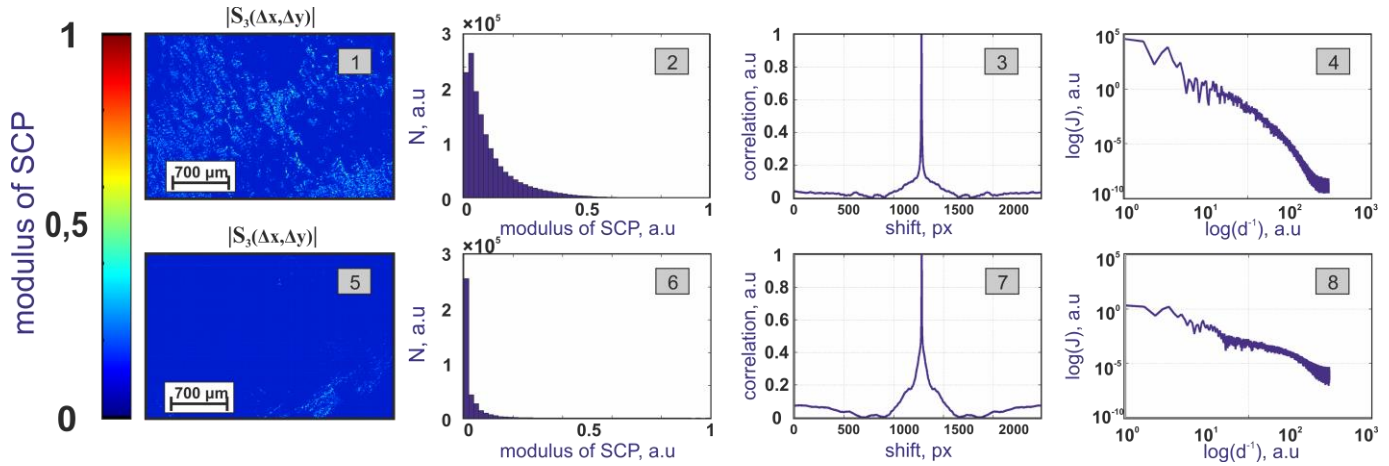

Fig.3. Maps (coordinate distributions (1), (5), histograms (2), (6), autocorrelation functions (3), (7), logarithmic dependences of power spectra (4), (8)) of SCP modulus $\left|S_{i=4}\left(\Delta x;\Delta y\right)\right|$ of polarization-inhomogeneous images of histological sections of a healthy ((1), (2), (3), (4)) and pathologically changed ((5), (6), (7), (8)) rat kidney. See explanations in the text.
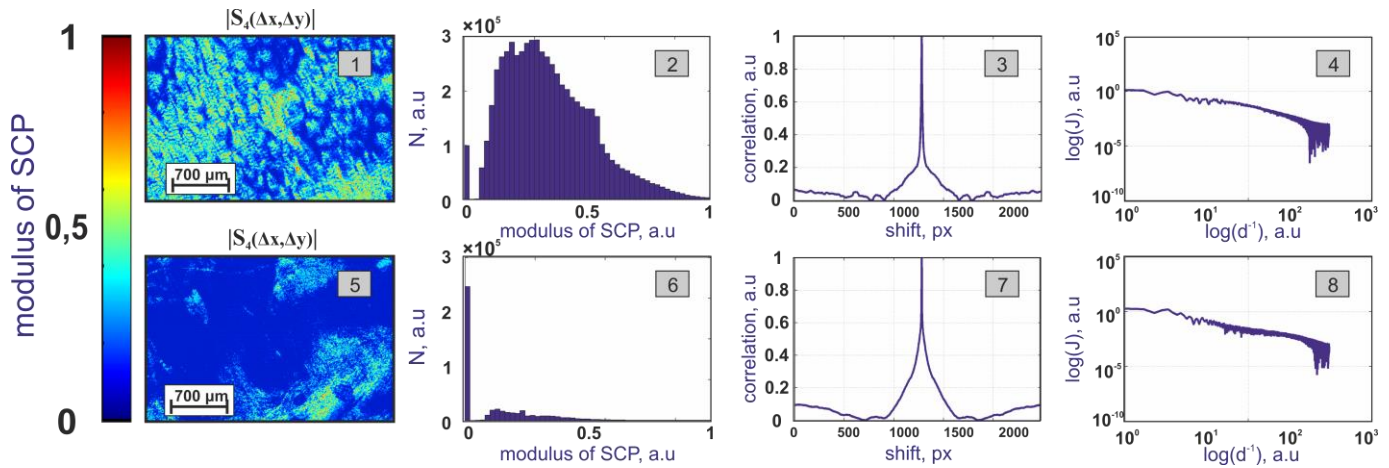
$$D^{f} = \sqrt{\frac{1}{N}\sum_{j=1}^{N}\left(\log J(q) - \log(\nu)^{2}\right)_{j}}.$$

(32)

IV. RESULTS AND DISCUSSION

A. SCP modulus and phase maps of polarization-inhomogeneous images of histological sections of rat kidney

To compare the theoretical (relations (16)-(23)) and experimental data, irradiation of samples of tissues of internal organs of rats was carried out by a plane-polarized beam with azimuth 0^{0} ($E_{0} = \begin{pmatrix} 1 \\ 0 \end{pmatrix}$).

Fig.2 and Fig.3 present the SCP-maps of the modulus $\left|S_{i=3}\left(\Delta x;\Delta y\right)\right|$ values distribution and $\left|S_{i=4}\left(\Delta x;\Delta y\right)\right|$ microscopic images of histological sections of a healthy and diabetic (21 days) rat kidney respectively.

In a same manner Fig.4 and Fig.5 are shows the SCP-maps of the phase $Arg\left(S_{i=3}\left(\Delta x;\Delta y\right)\right)$ and $Arg\left(S_{i=4}\left(\Delta x;\Delta y\right)\right)$ values distribution of microscopic images for healthy and diabetic kidney samples. Statistical analysis of SCP modulus $\left|S_{i=3;4}\left(\Delta x;\Delta y\right)\right|$ maps structure of polarization-inhomogeneous images for kidney samples of both types showed different localization of extremes and half-width of corresponding histograms $N\left(\left|S_{i=3;4}\left(\Delta x,\Delta y\right)\right|\right)$ (normal, see Fig.2 and Fig.3, fragments (2) and $N^{*}\left(\left|S_{i=3;4}\left(\Delta x,\Delta y\right)\right|\right)$), (diabetes, see Fig.2, Fig.3 fragments (6)). The obtained results can be explained by the following reasons. Due to weak phase modulation, the object field of the histological sections turns out to be sufficiently polarization-homogeneous with respect to the most probable value $E_{0} = \begin{pmatrix} 1 \\ 0 \end{pmatrix}$. According to the data presented in Table I, the most probable value in the distributions of the random magnitude of SCP orientation
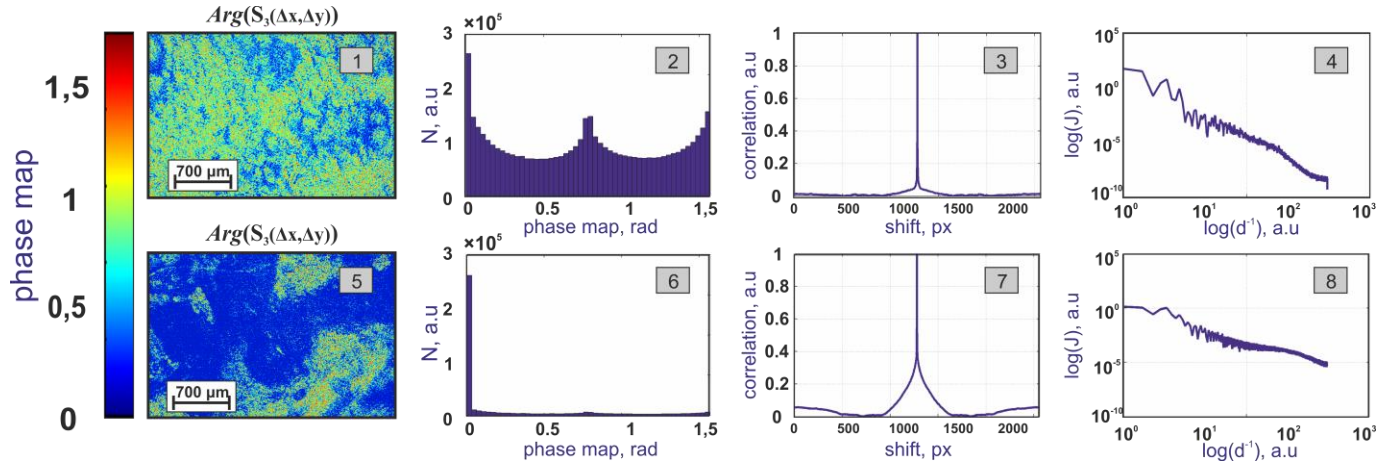
Fig.4. Maps (coordinate distributions (1), (5), histograms (2), (6), autocorrelation functions (3), (7), logarithmic dependences of power spectra (4), (8)) of SCP phase $Arg\big(S_{i=3}(\Delta x; \Delta y)\big)$ of polarization-inhomogeneous images of histological sections of a healthy ((1), (2), (3), (4)) and pathologically changed ((5), (6), (7), (8)) rat kidney. See explanations in the text.
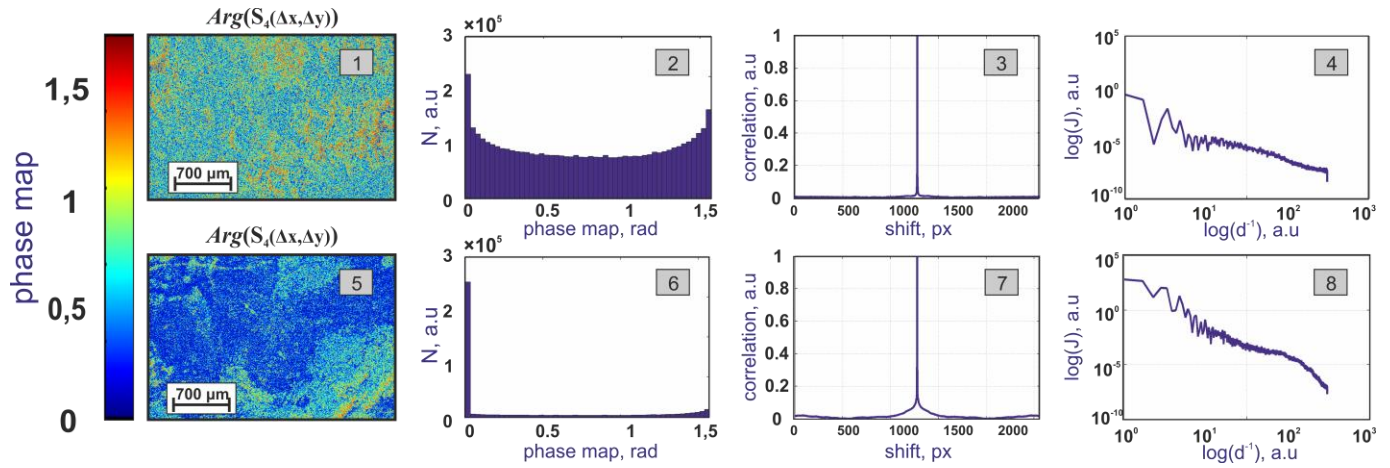

Fig.5. Maps (coordinate distributions (1), (5), histograms (2), (6), autocorrelation functions (3), (7), logarithmic dependences of power spectra (4), (8)) of SCP phase $Arg\big(S_{i=4}(\Delta x; \Delta y)\big)$ of polarization-inhomogeneous images of histological sections of a healthy ((1), (2), (3), (4)) and pathologically changed ((4), (5), (7), (8)) rat kidney. See explanations in the text.

maps turns out to be $\left|S_{i=3;4}(\Delta x, \Delta y)\right| = 1$. The SCP modulus $\left|S_{i=3;4}(\Delta x, \Delta y)\right|$ values (see Fig.2 and Fig.3, fragments (1), (5)) are primarily defined by the relations $\rho_{1;2}$ between the orthogonal parts of complex amplitudes of neighboring points r_1 and r_2 of the histological section plane (equations (22), (23)). In kidney tissue with spatially structured collagen fibrils network differences between the $\rho(r_1)$ and $\rho(r_2)$ are minor ($\rho(r_1) - \rho(r_2) \to 0$) for the neighboring points (the scanning step $\Delta r = 1pix = 2\mu m$). Thus, the following boundary values of modulus $\left|S_{i=3}(\Delta x, \Delta y)\right| \to 0$ (equation (22)) and $\left|S_{i=3}(\Delta x, \Delta y)\right| \to 0$ (equation (23)) are quite probable. So, they form the core extremes of histograms $N\big(\left|S_{i=3;4}(\Delta x, \Delta y)\right|\big)$ and $N^*\big(\left|S_{i=3;4}(\Delta x, \Delta y)\right|\big)$ (see Fig.2 and Fig.3, fragments (2), (6)). However, for real kidney tissue there is always a certain amount of curvilinear fibrils. For such birefringent networks

there is a condition $\rho(r_1) - \rho(r_2) \neq 0$. Thus, the set of other values of SCP modulus $\left|S_{i=3;4}(\Delta x, \Delta y)\right|$ is formed.

Quantitatively, this scenario appears in the redistribution of $\left|S_{i=3;4}(\Delta x, \Delta y)\right|$ values in the entire range $0 \leq \left|S_{i=3;4}(\Delta x, \Delta y)\right| \leq 1$ (see Fig.2 and Fig.3, fragments (2), (6)).

Additionally, the comparative intergroup analysis revealed the correlation coherence increment of polarization states at the points of images of diabetic samples. Analytically it was indicated by the reduction of half-width of histograms $N^*\big(\left|S_{i=3;4}(\Delta x; \Delta y)\right|\big)$ of the modulus $\left|S_{i=3;4}(\Delta x; \Delta y)\right|$ values distributions of the boundary field of diabetic kidney (see Fig.2 and Fig.3 fragments (6)).

The statistical structure of SCP phase maps is different. The value of $Arg\big(S_{3;4}(\Delta x, \Delta y)\big)$ (see Fig.4 and Fig.5, fragments (1), (5)) is simultaneously determined by the degree of coordinate coherence of parameters $\rho(r)$ and the value of

phase shift $\delta(r)$ between the orthogonal components of the amplitude of the laser radiation. It follows from the data analysis of relations that extreme values of $Arg(S_3(\Delta x, \Delta y)) \rightarrow 0$ and $Arg(S_4(\Delta x, \Delta y)) \rightarrow 0.5\pi$ are determined by fulfillment of these orientation and phase conditions $\Delta r = 2\mu m \rightarrow \begin{pmatrix} \rho(r_1) \approx \rho(r_2); \\ \delta(r_1) \approx \delta(r_2) \end{pmatrix}$ (see Table I).

Quantitatively, it is manifested in the prevailing probability of forming the values of histograms $N(Arg(S_3(\Delta x, \Delta y)) = 0)$ and $N(Arg(S_4(\Delta x, \Delta y)) = 0.5\pi)$ (see Fig.4 and Fig.5, fragments (2), (6)). However, this mechanism is not the only one. The phase shift value is also changes because of the difference in size of birefringent collagen fibrils and their curvilinearity.

TABLE II

STATISTICAL, CORRELATION AND FRACTAL PARAMETERS OF SCP MODULUS MAPS OF POLARIZATION-INHOMOGENEOUS IMAGES OF HISTOLOGICAL SECTIONS OF HEALTHY AND PATHOLOGICALLY CHANGED RAT KIDNEY

Parameters	$\|S_{i=3}(\Delta x, \Delta y)\|$		$\|S_{i=4}(\Delta x, \Delta y)\|$	
Condition	Norm $(n = 39)$	Diabetes $(n = 39)$	Norm $(n = 39)$	Diabetes $(n = 39)$
Z_1	0,027±0,0019	0,016±0,0011	0,74±0,034	0,089±0,004
Z_2	0,013±0,0011	0,007±0,0005	0,23±0,016	0,081±0,009
Z_3	1,35±0,12	3,78±0,24	0,69±0,055	2,07±0,19
Z_4	3,24±0,24	7,18±0,39	0,82±0,069	3,95±0,22
Z_2^k	0,07±0,005	0,11±0,009	0,06±0,005	0,09±0,007
Z_4^k	2,48±0,16	0,98±0,078	1,63±0,12	0,87±0,068
D^f	0,22±0,017	0,17±0,013	0,32±0,021	0,21±0,017

So, both of this factors has an influence on the wide range of SCP phase values ($0 \leq Arg(S_{i=3;4}(\Delta x, \Delta y)) \leq 0.5\pi$) in polarization-inhomogeneous image of the kidney histological section.

Intergroup analysis showed the decrease of the average and dispersion values characterizing the distributions of SCP phase $Arg(S_{i=3;4}(\Delta x; \Delta y))$ of polarization-inhomogeneous image of diabetic kidney samples (see Fig.4 and Fig.5 fragments (2), (6)).

From a physical point of view, the changes of the statistical structure of SCP-maps of polarization-inhomogeneous images for the kidney samples of both types can be explained by the fact that the pathological state (diabetes) is accompanied by the destruction of the organ tissue [4,7,18,19,24,26,27]. Optically, this process leads to the destruction of polycrystalline kidney structure while small-scale optically anisotropic structure remains intact. Thus, the polarization image uniformity of these tissues increases. Quantitatively, it is results in the increase of the probability of extreme values of $\|S_{i=3}(\Delta x; \Delta y)\| = 0$; $\|S_{i=4}(\Delta x; \Delta y)\| = 1$ and $Arg(S_{i=3}(\Delta x; \Delta y)) = 0$; $Arg(S_{i=4}(\Delta x; \Delta y)) = 0.5\pi$ in the distributions of the values of SCP modulus and phase. Therefore, higher order statistical moments that characterize the asymmetry and excess of SCP modulus and phase

distributions of the images of the sick kidneys sample are changed by the following scenario

$$\begin{cases} Z_3(\|S_{i=3;4}(\Delta x; \Delta y)\|; Arg(S_{i=3;4}(\Delta x; \Delta y)))\uparrow; \\ Z_4(\|S_{i=3;4}(\Delta x; \Delta y)\|; Arg(S_{i=3;4}(\Delta x; \Delta y)))\uparrow. \end{cases}$$ (33)

Autocorrelation dependences (Eqs.((30)-(31)) of coordinate distributions of SCP modulus and phase of the pathological kidney images are characterized by the increase of half-width and the decrease in peak sharpness

$$\begin{cases} Z_2^K(\|S_{i=3;4}(\Delta x; \Delta y)\|; Arg(S_{i=3;4}(\Delta x; \Delta y)))\uparrow; \\ Z_4^K(\|S_{i=3;4}(\Delta x; \Delta y)\|; Arg(S_{i=3;4}(\Delta x; \Delta y)))\downarrow. \end{cases}$$ (34)

TABLE III

STATISTICAL, CORRELATION AND FRACTAL PARAMETERS OF SCP PHASE MAPS OF POLARIZATION-INHOMOGENEOUS IMAGES OF HISTOLOGICAL SECTIONS OF HEALTHY AND PATHOLOGICALLY CHANGED RAT KIDNEY

Parameters	$Arg(S_{i=3}(\Delta x; \Delta y))$		$Arg(S_{i=4}(\Delta x; \Delta y))$	
Condition	Norm $(n = 39)$	Diabetes $(n = 39)$	Norm $(n = 39)$	Diabetes $(n = 39)$
Z_1	0,018±0,0013	0,012±0,001	0,91±0,051	0,15±0,012
Z_2	0,12±0,017	0,046±0,0032	0,14±0,015	0,074±0,003
Z_3	0,64±0,054	1,95±0,13	0,56±0,043	1,79±0,14
Z_4	0,78±0,061	4,09±0,33	0,67±0,051	3,29±0,27
Z_2^k	0,06±0,005	0,1±0,009	0,05±0,005	0,07±0,007
Z_4^k	3,64±0,16	1,48±0,078	4,61±0,12	2,37±0,068
D^f	0,24±0,017	0,15±0,013	0,28±0,021	0,19±0,017

It was determined in cases of the Stokes-correlometry mapping that the experimentally measured SCP-maps ($\|S_{i=3;4}(\Delta x, \Delta y)\|$ and $Arg(S_{i=3;4}(\Delta x; \Delta y))$) have fractal or multifractal structure. The approximating lines of the logarithmic dependences $\log J(\|S_{i=3;4}(\Delta x, \Delta y)\|) - \log(d^{-1})$ and $\log J(Arg(S_{i=3;4}(\Delta x, \Delta y))) - \log(d^{-1})$ are either straight or broken with two inclination angles (see Fig.2 – Fig.5, fragments (4), (8)). It follows from the comparative analysis of these dependences that the distributions of their values are characterized by a specific value of dispersion D^f (equation (32)). The smallest one is observed for a polarization-inhomogeneous image of the kidney tissue affected by diabetes. From a physical point of view, it can be related to peculiarity of geometric sizes of the structural elements of SCP-maps which are reduced due to degradation of optical anisotropy of the pathologically changed kidney.

The potentality of Stokes-correlometry differentiation of the two kidney groups is quantitatively illustrated by the data presented in Table II and Table III.

The procedure for differentiating specimens of histological sections of the kidney tissue consisted of:
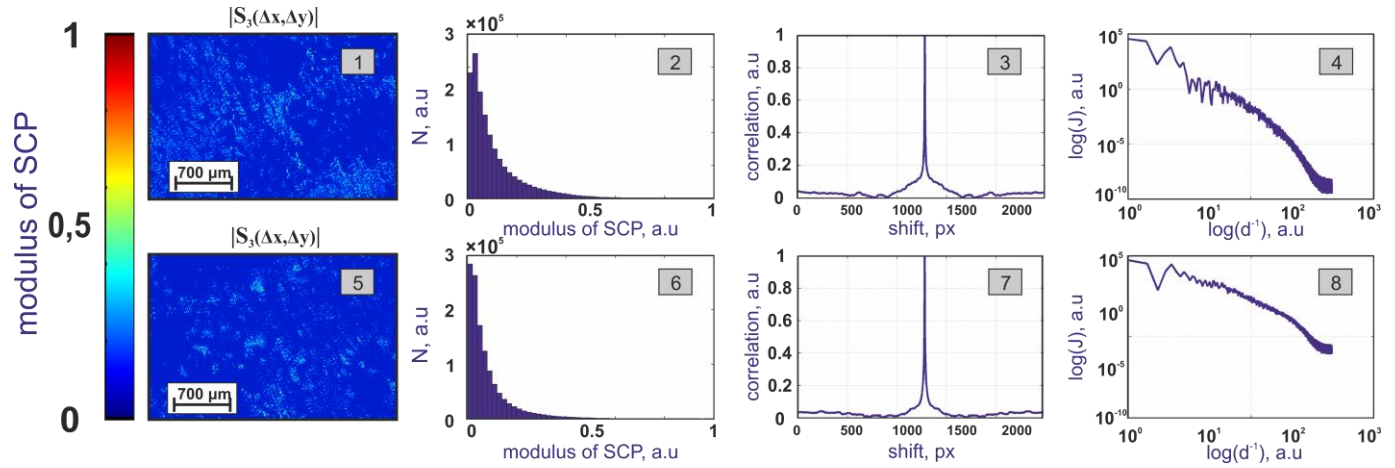
Fig.6. Maps (coordinate distributions (1), (5), histograms (2), (6) autocorrelation functions (3), (7), logarithmic dependences of power spectra (4), (8)) of SCP modulus $|S_{i=3}(\Delta x;\Delta y)|$ of polarization-inhomogeneous images of histological sections of a healthy ((1), (2), (3), (4)) and pathologically changed ((5), (6), (7), (8)) rat liver. See explanations in the text.
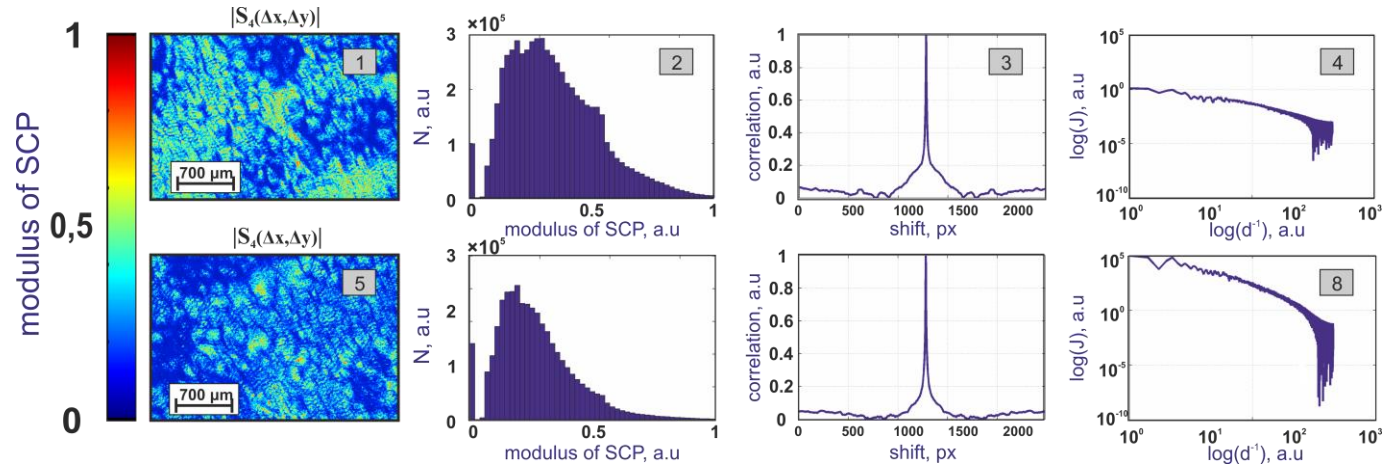

Fig.7. Maps (coordinate distributions (1), (5), histograms (2), (4) autocorrelation functions (3), (7), logarithmic dependences of power spectra (4), (8)) of SCP modulus $|S_{i=4}(\Delta x;\Delta y)|$ of polarization-inhomogeneous images of histological sections of a healthy ((1), (2), (5), (6)) and pathologically changed ((3), (4), (7), (8)) rat liver. See explanations in the text.

i. calculation of the set of objective parameters

$$P = \begin{pmatrix} Z_{i=1;2;3;4}; \\ Z_{i=2;4}^k; \\ D^f \end{pmatrix}$$ characterizing the distributions of the

modulus $|(S_{i=3;4}(\Delta x, \Delta y))|$ and the phase $Arg(S_{i=3;4}(\Delta x, \Delta y))$ of the SCP;

ii. detection of the maximal differences between the parameters P;

iii. calculation of the mean values $\overline{P}$ and their errors within a certain partial layer $\pm\sigma$ for each group of samples;

iv. search of the balanced accuracy $Ac,\%$ of the diagnostic test on the basis of the following relations determined for each group of samples [30-32]: sensitivity ($Se = \dfrac{a}{a+b}100\%$)

specificity ($Sp = \dfrac{c}{c+d}100\%$) and balanced accuracy

($Ac = \dfrac{Se+Sp}{2}$), where a and b are the number of correct and wrong diagnoses within group 2; c and d are the same numbers within group 1

The data analysis revealed the following differences between the set of objective parameters characterizing the maps of SCP-modulus of polarization-inhomogeneous images for the healthy and diabetic kidney samples:

- $\Delta Z_1 = 1.67 - 8.11$ times; $\Delta Z_2 = 1.85 - 2.83$ times; $\Delta Z_3 = 2.8 - 3$ times; $\Delta Z_4 = 2.21 - 4.81$ times;

- $\Delta Z_2^k = 1.5 - 1.57$ times; $\Delta Z_4^k = 1.87 - 2.53$ times;

- $\Delta D^f = 1.29 - 1.52$ times.

These data were obtained for the SCP phase distributions:

- $\Delta Z_1 = 1.51 - 6.06$ times; $\Delta Z_2 = 2.1 - 2.6$ times; $\Delta Z_3 = 3.04 - 3.19$ times; $\Delta Z_4 = 4.91 - 5.24$ times;

- $\Delta Z_2^k = 1.4 - 1.66$ times; $\Delta Z_4^k = 1.95 - 2.45$ times;

$\Delta D^f = 1.47 - 1.58$ times.

Maps of SCP modulus and phase of polarization-inhomogeneous images of rat liver histological sections

Fig.6 and Fig.7 show the SCP- maps of the distributions of modulus values $\left(S_{i=3}(\Delta x;\Delta y)\right)$ and $\left(S_{i=4}(\Delta x;\Delta y)\right)$ of microscopic images of liver parenchymatous tissue of the healthy and diabetic rats (21 days). Whereas, in Fig.8 and Fig.9 SCP- maps of the distributions of phase values $Arg\left(S_{i=3}(\Delta x;\Delta y)\right)$ and $Arg\left(S_{i=4}(\Delta x;\Delta y)\right)$ of microscopic images for the liver samples of the healthy and diabetic rat (21 days) are presented.

The combined analysis of the structure of SCP modulus $\left|S_{i=3;4}(\Delta x;\Delta y)\right|$ and phase $Arg\left(S_{i=3;4}(\Delta x;\Delta y)\right)$ of polarization-inhomogeneous fields liver samples of both healthy and diabetic types showed the same patterns for optically anisotropic manifestations of diabetes, as those found in the previous studies of the kidney images (see Fig.6 – Fig.9).

TABLE IV
STATISTICAL, CORRELATION AND FRACTAL PARAMETERS OF SCP MODULUS MAPS OF POLARIZATION-INHOMOGENEOUS IMAGES OF HISTOLOGICAL SECTIONS OF HEALTHY AND PATHOLOGICALLY CHANGED RAT LIVER.

Parameters	$\left|S_{i=3}(\Delta x;\Delta y)\right|$		$\left|S_{i=4}(\Delta x;\Delta y)\right|$	
Condition	Norm $(n=39)$	Diabetes $(n=39)$	Norm $(n=39)$	Diabetes $(n=39)$
Z_1	0.073±0,0047	0,058±0,0032	0,36±0,023	0,25±0,014
Z_2	0,15±0,012	0,11±0,005	0,32±0,016	0,21±0,013
Z_3	0,65±0,047	1,27±0,062	0,48±0,025	0,87±0,051
Z_4	0,54±0,034	1,42±0,079	0,56±0,039	0,79±0,037
Z_2^k	0,068±0,005	0,074±0,004	0,086±0,005	0,093±0,007
Z_4^k	2,58±0,16	3,88±0,21	1,13±0,061	0,78±0,059
D^f	0,22±0,019	0,17±0,015	0,33±0,023	0,24±0,016

TABLE V
STATISTICAL, CORRELATION AND FRACTAL PARAMETERS OF SCP PHASE MAPS OF POLARIZATION-INHOMOGENEOUS IMAGES OF HISTOLOGICAL SECTIONS OF HEALTHY AND PATHOLOGICALLY CHANGED RAT LIVER

Parameters	$Arg\left(S_{i=3}(\Delta x;\Delta y)\right)$		$Arg\left(S_{i=4}(\Delta x;\Delta y)\right)$	
Condition	Norm $(n=39)$	Diabetes $(n=39)$	Norm $(n=39)$	Diabetes $(n=39)$
Z_1	0,88±0,049	0,67±0,034	0,64±0,041	0,52±0,037
Z_2	1,16±0,062	0,82±0,057	1,04±0,061	0,72±0,045
Z_3	0,59±0,032	0,83±0,057	0,37±0,024	0,58±0,041
Z_4	0,89±0,053	1,37±0,071	0,62±0,042	0,96±0,051
Z_2^k	0,051±0,0031	0,072±0,006	0,028±0,003	0,036±0,005
Z_4^k	2,78±0,18	1,86±0,26	3,07±0,22	4,71±0,31
D^f	0,27±0,013	0,21±0,019	0,28±0,017	0,19±0,013

The differences between the statistical, correlation and fractal parameters describing the coordinate maps of SCP modulus and the phase of polarization-inhomogeneous images for liver samples are quantitatively illustrated in Table IV and Table V.

The obtained data analysis revealed the following differences between the set of objective parameters characterizing the maps of SCP modulus of polarization-

inhomogeneous images of kidney histological sections of the healthy and diabetic rat:

- $\Delta Z_1 = 1.26 – 1.44$ times; $\Delta Z_2 = 1.36 – 1.52$ times; $\Delta Z_3 = 1.81 – 1.95$ times; $\Delta Z_4 = 1.41 – 2.63$ times;
- $\Delta Z_2^k = 1.05 – 1.14$ times; $\Delta Z_4^k = 1.44 – 1.51$ times;
- $\Delta D^f = 1.29 – 1.37$ times.

It was obtained for the SCP phase distributions:

- $\Delta Z_1 = 1.23 – 1.31$ times; $\Delta Z_2 = 1.41 – 1.44$ times; $\Delta Z_3 = 1.41 – 1.57$ times; $\Delta Z_4 = 1.54 – 1.56$ times;
- $\Delta Z_2^k = 1.2 – 1.41$ times; $\Delta Z_4^k = 1.49 – 1.53$ times;
- $\Delta D^f = 1.29 – 1.47$ times.

The most sensitive data are marked with * in Tables VI and VII.

Comparing the results of statistical, correlation and fractal analyses of the maps of SCP modulus and phase of polarization-inhomogeneous images of the structured (kidney) and parenchymatous (liver) rat tissues, significant sensitivity to the changes in optical anisotropy of the "islet" parenchymatous structures has been found; the values of the objective parameters has a 2-fold difference.

TABLE VI
ACCURACY OF THE METHODS OF STOKES-CORRELOMETRY AND LASER POLARIMETRY OF RAT KIDNEY FIBRILLAR TISSUE IN THE DIFFERENTIAL DIAGNOSTICS OF DIABETES

Parameters	$Ac,\%$					
	$\left|S_3\right|$	$\left|S_4\right|$	$ArgS_3$	$ArgS_4$	$\alpha(x,y)$	$\beta(x,y)$
Z_1	90*	92*	96*	97*	65	68
Z_2	91*	90*	94*	96*	64	67
Z_3	92*	87	97*	95*	82	83
Z_4	90*	91*	95*	98*	80	81
Z_2^k	82	81	85	87	62	64
Z_4^k	93*	93*	98*	98*	83	82
D^f	80	82	84	86	67	68

TABLE VII
ACCURACY OF THE METHODS OF STOKES-CORRELOMETRY AND LASER POLARIMETRY OF RAT LIVER TISSUE IN THE DIFFERENTIAL DIAGNOSTICS OF DIABETES

Parameters	$Ac,\%$					
	$\left|S_3\right|$	$\left|S_4\right|$	$ArgS_3$	$ArgS_4$	$\alpha(x,y)$	$\beta(x,y)$
Z_1	85	83	92*	91*	63	65
Z_2	86	88	90*	92*	61	63
Z_3	84	82	91*	90*	79	78
Z_4	90*	90*	90*	92*	77	75
Z_2^k	78	77	80	81	58	59
Z_4^k	90*	90*	92*	92*	74	77
D^f	76	75	80	81	60	61

To determine the Stokes-correlometry diagnostic efficiency the obtained results were compared with the data obtained by conventional laser polarimetry for the same samples.
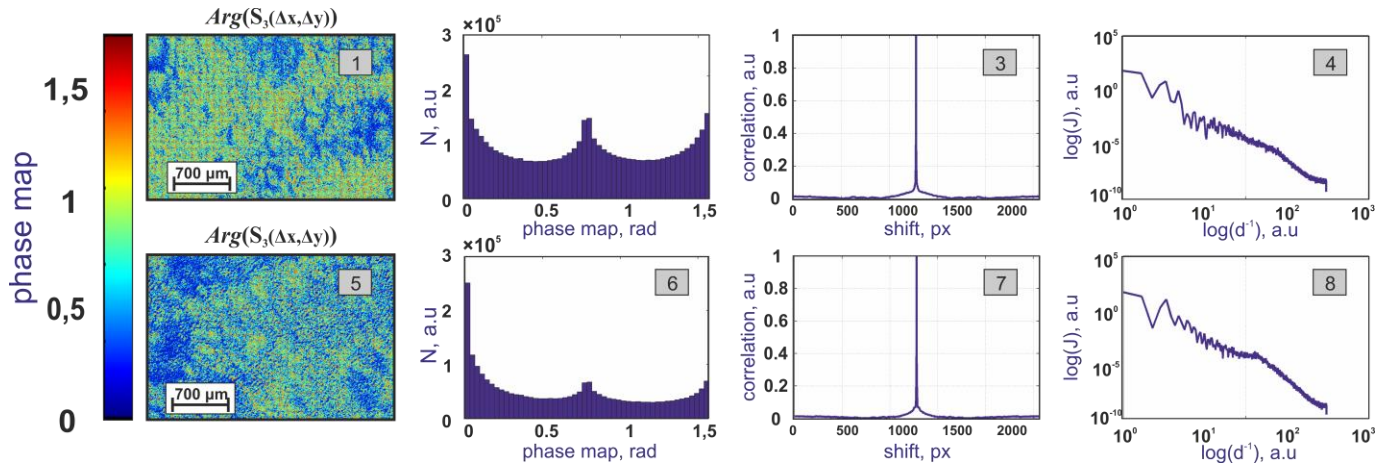
Fig.8. Maps (coordinate distributions (1), (5), histograms (2), (6) autocorrelation functions (3), (7), logarithmic dependences of power spectra (4), (8)) of SCP phase $Arg\left(S_{i=3}(\Delta x; \Delta y)\right)$ of polarization-inhomogeneous images of histological sections of a healthy ((1), (2), (3), (4)) and pathologically changed ((5), (6), (7), (8)) rat liver. See explanations in the text.
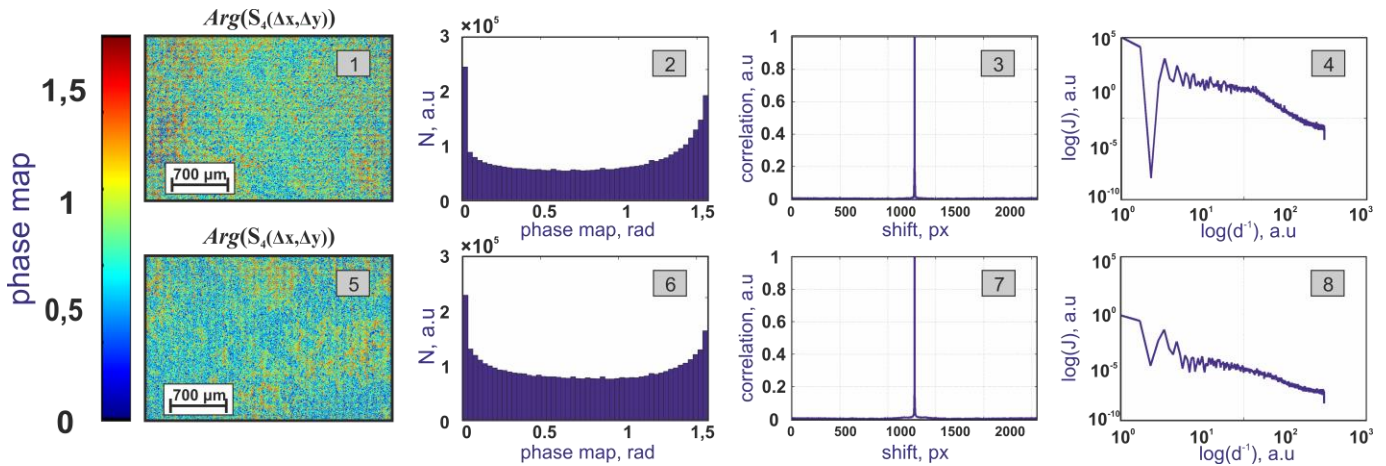

Fig.9. Maps (coordinate distributions (1), (5), histograms (2), (4) autocorrelation functions (3), (7), logarithmic dependences of power spectra (4), (8)) of SCP phase $Arg\left(S_{i=4}(\Delta x; \Delta y)\right)$ of polarization-inhomogeneous images of histological sections of a healthy ((1), (2), (5), (6)) and pathologically changed ((3), (4), (7), (8)) rat liver. See explanations in the text.

V. STOKES-CORRELOMETRY APPROACH

The Stokes-correlometry method of SCP modulus $\left|S_{i=3;4}(\Delta x; \Delta y)\right|$ and phase $Arg\left(S_{i=3;4}(\Delta x; \Delta y)\right)$ distributions of polarization-inhomogeneous images was compared with the that of polarization mapping of the azimuth and ellipticity values distributions for the corresponding microscopic images of kidney (Table VI) and liver (Table VII) samples (two healthy and two diabetic groups of rats, respectively).

The complex study showed significantly greater accuracy for the methods of Stokes-correlometry in the differentiation of weak changes in optical anisotropy of histological sections of the structured ($94\% \leq \max Ac \leq 98\%$) and parenchymatous ($90\% \leq \max Ac \leq 92\%$) biological tissues of internal organs of healthy and diabetic rats.

VI. CONCLUSIONS

A new diagnostic approach based on determination of the spatial distributions of the modulus and phase of 'two-point' Stokes-vector parameters of polarization-inhomogeneous images of histological sections of biological tissues with different morphological structures and physiological states has been introduced. The SCP-mapping of microscopy polarization images of two groups (normal and diabetic samples) of biological tissues with the structured collagen birefringent fibrillar networks (kidney), and with the 'islet' isotropic-anisotropic structure (liver) were examined. The combined use of statistical, correlation and fractal analysis of spatial distribution of 'single-point' azimuth and ellipticity and 'two-point' Stokes-vector parameters of polarization images of histological sections demonstrated the high accuracy

This article has been accepted for publication in a future issue of this journal, but has not been fully edited. Content may change prior to final publication. Citation information: DOI 10.1109/JSTQE.2018.2865443, IEEE Journal of Selected Topics in Quantum Electronics

> REPLACE THIS LINE WITH YOUR PAPER IDENTIFICATION NUMBER (DOUBLE-CLICK HERE TO EDIT) <   12

($Ac \geq 90\%$) in diagnosis of optical anisotropy variations within biological tissues.

REFERENCES

[1] T. Novikova, *et al.*, "Polarized Light for Biomedical Applications", *J. Biomed. Opt.*, Vol.21, 071001, 2016.

[2] N.G. Khlebtsov, *et al.*, "Introduction to Light Scattering by Biological Objects: Extinction and Scattering of Light in Disperse Systems", in: *Handbook of Optical Biomedical Diagnostics*, Ed. V. Tuchin, SPIE Press, (2016), Chapter 1.

[3] T.T. Tower, and R.T. Tranquillo, "Alignment Maps of Tissues: I. Microscopic Elliptical Polarimetry," *Biophys. J.*, vol. 81, pp. 2954–2963, 2001.

[4] A.G. Ushenko, and V.P. Pishak, "Laser Polarimetry of Biological Tissue: Principles and Applications," in *Handbook of Coherent-Domain Optical Methods: Biomedical Diagnostics, Environmental and Material Science*, Kluwer Academic Publishers, Vol.1, V.V. Tuchin, Ed., 2004, pp. 93-138.

[5] V.V. Tuchin, L. Wang, and D.A. Zimnyakov, *Optical Polarization in Biomedical Applications*, New York, USA, 2006.

[6] N. Ghosh, and I.A. Vitkin, "Tissue polarimetry: concepts, challenges, applications and outlook," *J. Biomed. Opt.*, vol. 16, pp. 110801, 2011.

[7] V.A. Ushenko, and M.S. Gavrylyak, "Azimuthally invariant Mueller-matrix mapping of biological tissue in differential diagnosis of mechanisms protein molecules networks anisotropy," *Proc. SPIE*, vol. 8812, pp.88120Y, 2013.

[8] V.O. Ushenko, *et al.*, "Two-dimensional Mueller matrix phase tomography of self-similarity birefringence structure of biological tissues," *Proc. SPIE*, vol. 8487, pp. 84870W, 2012.

[9] V.A. Ushenko, N. D. Pavlyukovich, and L. Trifonyuk, "Spatial-Frequency Azimuthally Stable Cartography of Biological Polycrystalline Networks," *In. J. Opt.*, pp. 683174, 2013.

[10] Yu.A. Ushenko, *et al.*, "Mueller-matrix diagnostics of optical properties of polycrystalline networks of human blood plasma," *Opt. Spectros.*, vol. 112, pp. 884-892, 2012.

[11] Yu.A. Ushenko *et al*, "Wavelet-analysis of polarization maps of human blood plasma," *Opt. Spectros.*, vol. 113, pp. 332-343, 2012.

[12] V.A. Ushenko, O.V. Dubolazov, and A.O. Karachevtsev, "Two wavelength Mueller matrix reconstruction of blood plasma films polycrystalline structure in diagnostics of breast cancer," *Appl. Opt.*, vol. 53, pp. B128-B139, 2014.

[13] A. Pierangelo, *et al.*, "*Ex-vivo* characterization of human colon cancer by Mueller polarimetric imaging," *Opt. Express*, 19, 1582-1593, 2011.

[14] N.K. Das, *et al.*, "Quantitative assessment of submicron scale anisotropy in tissue multifractality by scattering Mueller matrix in the framework of Born approximation", *Opt. Communications*, Vol.413, pp.172-178, 2018.

[15] N.K. Das, *et al.*, "Submicron scale tissue multifractal anisotropy in polarized laser light scattering", *Laser Phys. Lett.*, Vol.15, No.3, 035601, 2018.

[16] B. Kunnen, *et al.*, "Application of circularly polarized light for non-invasive diagnosis of cancerous tissues and turbid tissue-like scattering media", *J. Biophoton.*, Vol.8, No.4, pp.317 – 323, 2015.

[17] S.L. Jacques, "Polarized light imaging of biological tissues," in: *Handbook of Biomedical Optics*, CRC Press, Boca Raton, London, New York, D. Boas, C. Pitris, and N. Ramanujam, Eds., 2011, pp. 649–669.

[18] O.V. Angelsky *et al.*, "Statistical, Correlation and Topological Approaches in Diagnostics of the Structure and Physiological State of Birefringent Biological Tissues," in *Handbook of Photonics for Biomedical Science*, CRC Press, Taylor&Francis group: Boca Raton, London, New York, V.V. Tuchin, Ed. 2010, pp.283-322.

[19] Y.A. Ushenko, *et al.*, "Diagnostics of Structure and Physiological State of Birefringent Biological Tissues: Statistical, Correlation and Topological Approaches," in *Handbook of Coherent-Domain Optical Methods*, Springer Science+Business Media New York, 2013, pp.107-148.

[20] J. Ellis and A. Dogariu, "Complex degree of mutual polarization," *Opt. Lett.* vol. 29, pp. 536-538, 2004.

[21] V.P. Prysyazhnyuk *et al.*, "Polarization-dependent laser autofluorescence of the polycrystalline networks of blood plasma films in the task of liver pathology differentiation," *Appl. Opt.*, vol. 55, pp. B126-B132, 2016.

[22] A.V. Dubolazov, *et al.*, "Birefringence images of polycrystalline films of human urine in early diagnostics of kidney pathology," *Appl. Opt.* vol. 55, pp. B85-B90, 2016.

[23] Yu.A. Ushenko, *et al.*, "Spatial-frequency Fourier polarimetry of the complex degree of mutual anisotropy of linear and circular birefringence in the diagnostics of oncological changes in morphological structure of biological tissues," *Quantum. Electron.*, vol. 42, pp. 727–732, 2012.

[24] V.A. Ushenko, *et al.*, "Complex degree of mutual coherence of biological liquids," *Proc. SPIE*, vol. 8882, pp. 88820V, 2013.

[25] V.A. Ushenko, and M.P. Gorsky, "Complex degree of mutual anisotropy of linear birefringence and optical activity of biological tissues in diagnostics of prostate cancer," *Opt. Spectrosc.*, vol. 115, pp. 290-297, 2013.

[26] Yu.A. Ushenko, *et al.*, "Jones-matrix mapping of complex degree of mutual anisotropy of birefringent protein networks during the differentiation of myocardium necrotic changes," *Appl. Opt.*, vol. 55, pp. B113-B119, 2016.

[27] J. Tervo, T. Setala, and A. Friberg, "Degree of coherence for electromagnetic fields," *Opt. Expr.*, vol. 11, pp. 1137-1143, 2003.

[28] J. Tervo, T. Setala, and A. Friberg, "Two-point Stokes parameters: interpretation and properties," *Opt. Lett.*, vol. 34, pp. 3074-3076, 2009.

[29] V.V. Tuchin, *Tissue Optics: Light Scattering Methods and Instruments for Medical Diagnostics*, 3rd ed., Vol. PM 254, SPIE Press, Bellingham, Washington, 2015.

[30] L.D. Cassidy, "Basic concepts of statistical analysis for surgical research," *J. Surg. Res*., vol. 128, pp. 199-206, 2005.

[31] C.S. Davis, Statistical methods of the analysis of repeated measurements, New York: Springer-Verlag, 2002.

[32] A. Petrie and B. Sabin, *Medical Statistics at a Glance*, Blackwell Publishing, 2005, pp. 157.

Alexander Ushenko is a Professor at the Chernivtsi National University, Head of Optics and Publishing Department. He received his BSc and MSc degrees in Optics at the Chernivtsi State University in 1975 and 1977, respectively, and PhD degree in Optics and Laser Physics from the Chernivtsi State University in 1983. In 2000 he obtained D.Sc. in Optics and Laser Physics. He is the author of more than 200 journal papers, 60 patents and 20 monographies. His current research interests include laser polarimetry, polarization interferometry and digital holography.

Anton Sdobnov studied in Saratov State University, the Physical Faculty, Department of Optics and Biophotonics, where he completed his Master's degree in 2013 (diploma with honors). From 2013 to 2016 he worked as an engineer at the Physics Department in Saratov State University. Since 2016 he is a PhD student in the Optoelectronics and Measurement Techniques Unit of the University of Oulu, Finland. His main research interests are focused on the speckle contrast imaging, biophysics, and tissue optical clearing. Mr. Sdobnov was a recipient of the CIMO Scholarship in 2016 and EDUFI Scholarship in 2017.

Alexander Dubolazov is Associate Professor at the Chernivtsi National University. He received his BSc and MSc degrees in optics at the Chernivtsi National University in 2006 and 2007, respectively, and PhD degree in Optics and Laser Physics from the Chernivtsi National University in 2010. He is the author of more than 100 journal papers and 5 book chapters. His current research interests include laser polarimetry, holography.

Maryana Grytsiuk has graduated from the Medical Faculty in General Medicine of the Bukovinian State Medical Academy in 2003. In 2003-2004, she specialized as an intern in therapy at the Bukovinian Regional Clinical Hospital. In 2003 she had entered postgraduate studies in specialty Pathological Physiology at the Department of Medical Biology, Genetics and Histology, which she successfully graduated in 2006 with PhD degree. Since 2016 she is a Head of the Department of Social Medicine and Public Health of the Bukovinian State Medical University.

Yuriy Ushenko is a Professor at the Chernivtsi National University, Head of the Department of Computer Science. He received his BSc and MSc degrees in Biomedical Optics at the Chernivtsi National University in 2001 and 2003, respectively, and PhD degree in Optics and Laser Physics from the Chernivtsi National University in 2006. In 2015 he obtained D.Sc. in Optics and Laser Physics. He is the author of more than 150 journal papers, 30 patents and 9 monographies. His current research interests include laser polarimetry, polarization interferometry and digital holography.

Alexander Bykov is a senior research fellow/Adj. Prof. in the Optoelectronics and Measurement Techniques Unit, University of Oulu, Finland. He received his PhD in 2008 from Lomonosov Moscow State University, Russia. In 2010 he received his DSc (Tech.) degree from the Faculty of Technology, University of Oulu, Finland. He has published over 85 scientific peer-reviewed papers, 3 book chapters; over 45 presentations at the international conferences, including 13 invited lectures. His scientific interests are in the area of biophotonics, noninvasive optical diagnostics, theory of light propagation in scattering media including biotissues and numerical simulation of light transport.

Igor Meglinski, MSc, PhD, is a Professor, head of Biophotonics research at the University of Oulu, Finland. He received his PhD in Biophysics and Biomedical Optics at the interface between University of Pennsylvania, USA and Saratov State University, Russia in 1997. He is author and co-author of over 300 research papers in peer-reviewed scientific journals, proceedings of international conferences and book chapters, over 600 presentations at the major international conferences and symposia, including about 280 invited lectures, keynote and plenary talks. He is Chartered Physicist (CPhys) and Chartered Engineer (CEng), Fellow of the Institute of Physics (London, UK), Fellow of SPIE and Senior Memebr of IEEE. His research interests lie at the interface between physics, medicine, and biological sciences, focusing on the development of new non-invasive imaging/diagnostic techniques and their application in medicine and biology, material sciences, pharmacy, food, environmental monitoring, and health care industries.